AFRL-RQ-WP-TP-2013-0244

COMPENSATION METHOD FOR THE ESTIMATION OF THE AUTOSPECTRAL DENSITY FUNCTION OF THE UNEVENLY SPACED HIFiRE-1 FLIGHT DATA (POSTPRINT)

Scott A. Stanfield

Spectral Energies, LLC

Roger L. Kimmel

Hypersonic Sciences Branch
High Speed Systems Division

JUNE 2013

STINFO COPY

AIR FORCE RESEARCH LABORATORY
AEROSPACE SYSTEMS DIRECTORATE
WRIGHT-PATTERSON AIR FORCE BASE, OH 45433-7542
AIR FORCE MATERIEL COMMAND
UNITED STATES AIR FORCE

NOTICE AND SIGNATURE PAGE

*//Signature//   //Signature//
ROGER L. KIMMEL   MARK AMENDT, Chief
Project Manager   Hypersonic Sciences Branch
Hypersonic Sciences Branch   High Speed Systems Division
High Speed Systems Division   Aerospace Systems Directorate

REPORT DOCUMENTATION PAGE

Form Approved
OMB No. 0704-0188

The public reporting burden for this collection of information is estimated to average 1 hour per response, including the time for reviewing instructions, searching existing data sources, searching existing data sources, gathering and maintaining the data needed, and completing and reviewing the collection of information. Send comments regarding this burden estimate or any other aspect of this collection of information, including suggestions for reducing this burden, to Department of Defense, Washington Headquarters Services, Directorate for Information Operations and Reports (0704-0188), 1215 Jefferson Davis Highway, Suite 1204, Arlington, VA 22202-4302. Respondents should be aware that notwithstanding any other provision of law, no person shall be subject to any penalty for failing to comply with a collection of information if it does not display a currently valid OMB control number. **PLEASE DO NOT RETURN YOUR FORM TO THE ABOVE ADDRESS.**

1. REPORT DATE *(DD-MM-YY)* June 2013	2. REPORT TYPE Conference Paper Postprint	3. DATES COVERED *(From - To)* 30 June 2012 – 30 June 2013	
4. TITLE AND SUBTITLE COMPENSATION METHOD FOR THE ESTIMATION OF THE AUTOSPECTRAL DENSITY FUNCTION OF THE UNEVENLY SPACED HIFiRE-1 FLIGHT DATA (POSTPRINT)		5a. CONTRACT NUMBER In-house	
		5b. GRANT NUMBER	
		5c. PROGRAM ELEMENT NUMBER 61102F	
6. AUTHOR(S) Scott A. Stanfield (Spectral Energies, LLC) Roger L. Kimmel (AFRL/RQHF)		5d. PROJECT NUMBER 2307	
		5e. TASK NUMBER	
		5f. WORK UNIT NUMBER Q042	
7. PERFORMING ORGANIZATION NAME(S) AND ADDRESS(ES) Spectral Energies, LLC	Hypersonic Sciences Branch (AFRL/RQHF) High Speed Systems Division, Air Force Research Laboratory Aerospace Systems Directorate Wright-Patterson Air Force Base, OH 45433-7542 Air Force Materiel Command, United States Air Force	8. PERFORMING ORGANIZATION REPORT NUMBER AFRL-RQ-WP-TP-2013-0244	
9. SPONSORING/MONITORING AGENCY NAME(S) AND ADDRESS(ES) Air Force Research Laboratory Aerospace Systems Directorate Wright-Patterson Air Force Base, OH 45433-7542 Air Force Materiel Command United States Air Force		10. SPONSORING/MONITORING AGENCY ACRONYM(S) AFRL/RQHF	
		11. SPONSORING/MONITORING AGENCY REPORT NUMBER(S) AFRL-RQ-WP-TP-2013-0244	

12. DISTRIBUTION/AVAILABILITY STATEMENT
Approved for public release; distribution unlimited.

13. SUPPLEMENTARY NOTES
PA Case Number: 88ABW-2013-2541; Clearance Date: 04 Jun 2013. This paper contains color. The conference paper was presented at the 43rd Fluid Dynamics Conference, held in San Diego, California, from June 24 through 27, 2013, and was published in the AIAA Proceedings of the 43rd Fluid Dynamics Conference.

The U.S. Government is joint author of the work and has the right to use, modify, reproduce, release, perform, display, or disclose the work.

14. ABSTRACT
The time series data collected during the HIFiRE-1 flight experiment was sampled unevenly due to telemetry dropouts and the sampling scheme selected. Sampling unevenly results in frequency translation of power to artificial sidelobes. These sidelobes distort the real and imaginary components of the Fourier transform such that the spectrum of the sampled data no longer represents the spectrum of the physical process generating the data. These sidelobes can be eliminated by resampling the data onto an evenly spaced grid at the cost of under predicting the power of the higher frequency components in the data. In this paper, a compensation procedure is developed to recover the power loss caused by resampling. This compensation procedure is suitable for stochastic time series data having red-noise spectra such as the pressure fluctuations recorded underneath laminar and turbulent boundary layers.

15. SUBJECT TERMS
boundary layer transition, hypersonic, flight test

16. SECURITY CLASSIFICATION OF:			17. LIMITATION OF ABSTRACT: SAR	18. NUMBER OF PAGES 28	19a. NAME OF RESPONSIBLE PERSON (Monitor) Roger L. Kimmel
a. REPORT Unclassified	b. ABSTRACT Unclassified	c. THIS PAGE Unclassified			19b. TELEPHONE NUMBER *(Include Area Code)* N/A

Standard Form 298 (Rev. 8-98)
Prescribed by ANSI Std. Z39-18

Compensation Method for the Estimation of the Autospectral Density Function of the Unevenly Spaced HIFiRE-1 Flight Data

Scott A. Stanfield[1]
Spectral Energies, LLC, Dayton, OH, 45431

and

Roger L. Kimmel[2]
Air Force Research Laboratory, WPAFB, OH, 45433

The time series data collected during the HIFiRE-1 flight experiment was sampled unevenly due to telemetry dropouts and the sampling scheme selected. Sampling unevenly results in frequency translation of power to artificial sidelobes. These sidelobes distort the real and imaginary components of the Fourier transform such that the spectrum of the sampled data no longer represents the spectrum of the physical process generating the data. These sidelobes can be eliminated by resampling the data onto an evenly spaced grid at the cost of under predicting the power of the higher frequency components in the data. In this paper, a compensation procedure is developed to recover the power loss caused by resampling. This compensation procedure is suitable for stochastic time series data having red-noise spectra such as the pressure fluctuations recorded underneath laminar and turbulent boundary layers.

Nomenclature

a_i = regression coefficient

a_{50} = overlap correlation constant

b_i = regression coefficient

c_{xy} = coherency

D = location data point of a partition

f = frequency, Hz

---

[1] Research Scientist, AIAA Member.
[2] Senior Research Engineer, AFRL, Associate Fellow.

Approved for public release; distribution unlimited.

f_0 = fundamental frequency, Hz

f_c = Nyquist frequency, Hz

G_{xx} = autospectrum, Pa^2 / Hz

G_{xy} = cross-spectrum, Pa^2 / Hz

K = number of partitions

K_{eff} = effective number of partitions

L = number of data samples in a partition

N = number data samples in a time series

R = sum of squares

t = time, sec

t_f = time used to account for different time origins of time series used in cross spectral analysis, sec

t_L = time at the end of a partition, sec

T_p = period, sec

T_R = sampling interval, sec

w_n = Hanning window function coefficients

y_n = time series data

σ^2 = variance

τ = time shift, sec

ω = angular frequency, rad

I. Introduction

THE Hypersonic International Flight Research Experimentation (HIFiRE) program is a hypersonic flight test program executed by the Air Force Research Laboratory (AFRL) and the Australian Defence Science and Technology Organisation (DSTO).[1, 2] Its purpose is to develop and validate technologies critical to next generation hypersonic aerospace systems. Candidate technology areas include, but are not limited to, propulsion, propulsion-airframe integration, aerodynamics and aerothermodynamics, high temperature materials and structures, thermal management strategies, guidance, navigation, and control, sensors, and system components such as munitions, submunitions and avionics. The HIFiRE program consists of extensive ground tests and computation focused on specific hypersonic flight technologies. Each technology program is designed to culminate in a flight test.

The first science flight of the program, designated as HIFiRE-1, launched March 22, 2010 at Woomera Prohibited Area, Australia.[3] This flight was dedicated to two aerothermal experiments including laminar-turbulent boundary-layer transition on a 7-degree half-angle cone with nose bluntness of 2.5 mm and turbulent shock-boundary-layer interaction on a 33-degree flare/cylinder configuration. Prior to flight, a series of experimental and numerical studies were performed to aid the design of the aerothermal experiments such as sensor selection and placement, and vehicle geometry and materials.[4-15]

Approved for public release; distribution unlimited.

The cone, cylinder, and flare surfaces of the HIFiRE-1 payload were instrumented with many thermocouples, heat transfer gauges, and pressure transducers. During flight, the data from these transducers were digitized using a sampling scheme with a non-constant time interval between samples. This sampling scheme was used in order to achieve maximum stable throughput for a variety of sensors on a single flight computer. Although this sampling scheme maximized data acquisition, special care must be taken when performing spectral analysis on such unevenly-sampled data. This was especially true for the HIFiRE-1 high-bandwidth pressure data that were sampled at rates up to 60 kHz. In addition to the sampling scheme, random data dropouts sometimes occurred in the telemetry. Generally, these events were infrequent, and the dominant feature of data sampling was the uneven sampling rate. The current paper summarizes the methods used to analyze the high bandwidth pressure data, and quantifies spectral error introduced by uneven sampling.

A system consisting of a transducer, antialiasing filter, and sampling scheme is inherently nonlinear even though the transducers and antialiasing filters were linear devices. This nonlinearity is a direct consequence of the mutual dependence between frequencies in the frequency space of unevenly sampled time series data, and is dependent on only the sampled times. The spectral analysis of data measured by such a system is inherently complicated and requires special methods such as least squares,[17-22] interpolation,[23] slotted resampling,[24, 25] or continuous time models.[26, 27] Approaches based on these methods have been extensively studied and developed in other disciplines such as astronomy,[17-20] paleoclimatology,[21] seismology,[28] biomedical engineering,[29, 30] genetics,[31] and laser Doppler velocimetry.[24]

The least squares method, also referred to as the Lomb-Scargle method, determines the Fourier transform by estimating the different sinusoidal components of a time series. While more complicated to develop, the least squares method is robust requiring very little user input, and can be applied to any arbitrary sampling scheme including random sampling. Moreover, the least squares approach has been shown to be more fundamental than the traditional Fourier methods since, for evenly sampled time series data, the two methods are exactly identical. For unevenly sampled time series data, the two methods are identical within the numerical error generated when estimating the Fourier transform by numerical integration. As mentioned, the spectral distortion caused by sampling unevenly is independent of the data and depends only on the sampling scheme. Therefore, estimating the power spectrum from unevenly sampled data results a distorted spectrum that does not necessarily represent the spectrum of the physical process. The least squares method is not suitable for stochastic time series data with red-noise spectra such as the surface pressure fluctuations underneath a laminar or turbulent boundary layer because the analysis yields a distorted spectrum. The method can be useful for accurately computing the Fourier transform of unevenly sampled, sinusoidal periodic, complex periodic, and almost periodic data. There are some periodic data recorded during the HIFiRE-1 flight experiment for which the least squares method is the preferred method for computing the Fourier transform.

In general, the results obtained using interpolation methods, slotted resampling methods, and continuous time models introduce unwanted distortion, are not robust, and can require significant user input that is dependent on the nature of the time series. Specifically, interpolating methods such as nearest neighbor or spline interpolation are known to cause an underestimate of high frequency components independent of the employed interpolation scheme.[20, 21, 23] Moreover, results obtained using kernel based interpolation methods are dependent on the interpolation kernel and kernel parameters selected such as sinc, Gaussian, Laplacian, or rectangular kernels, and bandwidth, mainlobe width, and window width kernel parameters.[16] Unlike the least squares method, these methods are useful for estimating the spectral content of unevenly sampled, stochastic signals having red-noise spectra.

The use of slotted resampling, which estimates the autocorrelation function by summing the product pairs $X_i X_j$ into bins lagged by $t_i - t_j$, cannot be employed for an arbitrary sampling scheme since sufficiently large gaps in the data can cause the method to fail. These gaps could be filled in using interpolation. The interpolation process, if needed, and the binning process both independently contribute unwanted distortion to the time series data. Regardless of these negative attributes, the slotted resampling method may be a useful method for analyzing the HIFiRE-1 data. The use of this method for analyzing the HIFiRE-1 data is still under investigation and will not be discussed further in this paper.

The objective of this paper is to identify and outline a method capable of accurately estimating the autospectral density function from the unevenly sampled, surface pressure data underneath laminar, turbulent, and shock-influenced boundary layers collected during the HIFiRE-1 flight experiment. This objective requires some background information, which is developed prior to outlining an estimation procedure for the autospectral density function. In Section II, sampling theory is developed for unevenly sampled time series data. Several useful tools are identified from this development including the spectral window function and an alternate definition of the Nyquist frequency that holds for unevenly sampled time series data. Additionally, the nonlinear nature of the measurement and the source of the distortion in the Fourier transform of unevenly sampled measurements are

Approved for public release; distribution unlimited.

discussed. In Section III, the discussion applies the methodology developed in Section II to identify the nature of the HIFiRE-1 sampling scheme. The Nyquist frequencies for the unevenly sampled, surface pressure data recorded during the flight experiment are given and compared to the cutoff frequencies of the antialiasing filters. The range in frequencies without distortion, and thus suitable for analysis, is identified for each high bandwidth pressure transducer. In Section IV, the effects of resampling the unevenly spaced time series data onto an evenly spaced grid via linear interpolation are discussed. In this section, it is shown that resampling simplifies the process for estimating the autospectral density function of unevenly sampled data by replacing the distortion caused by the nonlinear sidelobes with an underestimate in power of the higher frequencies in the autospectral density function. In Section V, a compensation procedure is outlined for recovering the power loss caused by resampling. This compensation method is suitable for estimating the autospectral density function of stochastic time series data having red-noise spectra such as the surface pressure fluctuations recorded underneath laminar and turbulent boundary layers during the HIFiRE-1 flight experiment.

II.   Sampling Theory

A block diagram representing the sampling process of a continuous function is given in Fig. 1. In Fig. 1, the signal $x(t)$ represents the output from a measurement device such as a pressure transducer and is a continuous function, $x'(t)$ is a band limited function assumed to have the same amplitude and phase spectrum as $x(t)$ for frequencies below the cutoff frequency of the antialiasing filter, $s(t)$ is the sampling function, and $y(t_n)$ is a set of discrete samples of $x'(t)$ sampled at times t_n. The function $x(t)$ is filtered before sampling so that the frequency content of $x'(t)$ is limited to frequencies below the Nyquist frequency, defined as

$$f_c = \frac{1}{2\Delta t} \tag{1}$$

where Δt represents the sampling interval. According to the sampling theorem, $x'(t)$ can be reconstructed from $y(t_n)$ without information loss or distortion if the sampling rate is greater than or equal to twice the Nyquist frequency. If the sampling rate is less than twice the Nyquist frequency, spectral leakage from frequencies greater than the Nyquist frequency wrap-around and combine with the frequency content of frequencies below the Nyquist frequency. This problem is known as aliasing and in general cannot be removed.

The sampling function is defined as

$$s(t) = C \frac{\sum_{n=1}^{N} w_n \delta(t-t_n)}{\sum_{n=1}^{N} w_n} \tag{2}$$

where $\delta(t - t_n)$ is the Dirac delta function, t_n are the sampled times, N is the number of data points, and C and w_n are constants. The discrete signal $y(t_n)$ is given as

$$y(t_n) = s(t)x'(t) = \frac{1}{N}\sum_{n=1}^{N} x'(t_n)\delta(t - t_n) \tag{3}$$

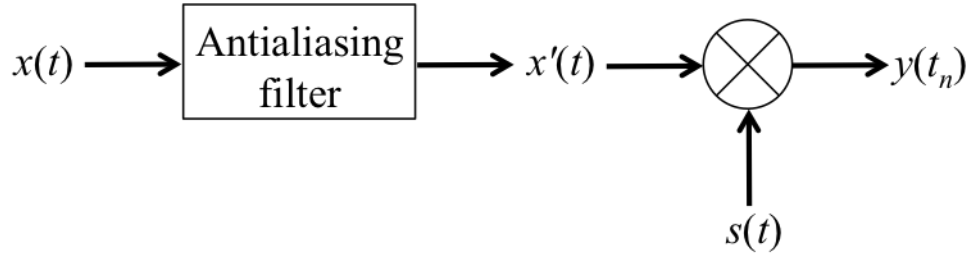where the constants C and w_n were set equal to 1. The discrete Fourier transform of Eq. 3 is given as

$$Y(f) = S(f) * X'(f) \tag{4}$$

where the Fourier transform is defined as

$$Y(f_k) = \int_{-\infty}^{\infty} y(t)e^{2\pi f_k t}dt \approx \sum_{n=0}^{N-1} y_n\, e^{2\pi i f_k t_n}\Delta t. \tag{5}$$

Typically, the sampling interval is moved outside the summation because it is constant for an evenly sampled time series. In this paper, the sampling interval is not necessarily constant and the sampling interval is left within the summation. In Eq. 4, $Y(f)$ is the Fourier transform of $y(t_n)$, $X'(f)$ is the Fourier transform of $x'(t_n)$, and $S(f)$ is the Fourier transform of $s(t)$ and is referred to as the normalized spectral window function. According to Eq. 4, and as pointed out by Deeming[32], "the pathology of the data distribution is all contained in the spectral window, which

4
Approved for public release; distribution unlimited.

can be calculated from the data spacing alone, and does not depend directly on the data themselves." The discussion will now focus on identifying the source of the distortion in the Fourier transform of unevenly sampled time series data using the normalized spectral window function.

Figure 1. Block diagram depicting the sampling process of a continuous function.

The power spectrum of the spectral window function, defined as $|S(f)|^2$, is shown in Fig. 2 for an evenly sampled time series with a sample rate of 100 Hz. From Fig. 2, the normalized spectral window function has peaks with amplitude of 1 centered at $2nf_c$ where $n = 0, 1, 2 \ldots \infty$. Hence, the normalized spectral window function is a periodic function with period $2f_c$. This periodicity is independent of the sample rate.

The power spectrum of the normalized spectral window function for an unevenly sampled time series sampled at a sampling rate of 200 Hz but with gaps in the data is shown in Fig. 3a. The power spectrum in Fig. 3a is similar to the power spectrum in Fig. 2 with peaks centered at $2nf_c$, however, there are additional peaks centered at 2, 6, and 10 Hz, as shown in Fig. 3b. These additional peaks are commonly referred to as sidelobes. The magnitude and location of the sidelobes are dependent on the sampling scheme. As will be shown, these sidelobes cause the real and imaginary components of $Y(f)$ and $X'(f)$ to be different. This difference is referred to within this paper as the distortion in $Y(f)$ caused by the sampling scheme.

The period of the spectral window function for an unevenly sampled time series is approximately $2f_c$, as shown in Fig. 3a. The spectral window function of an unevenly sampled time series is not always exactly periodic, as the peaks centered at $2nf_c$ for $n > 0$ are sometimes split into multiple peaks. The separation in frequency of the split peaks is very small such that the peaks are centered at approximately $2nf_c$. The center of the peak(s) at $2nf_c$ is used to determine the Nyquist frequency of an unevenly sampled time series since Eq. 1 is not valid when the sampling interval is not constant[33]. The meaning of the Nyquist frequency determined from the spectral window function is unchanged *i.e.* signals with non-zero amplitudes at frequencies exceeding the Nyquist frequency wrap-around polluting the Fourier transform at frequencies below the Nyquist frequency.
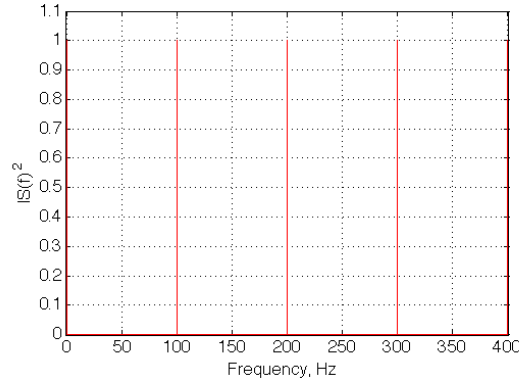
There is an additional unwanted artifact caused by aliasing that is inherent only to unevenly sampled time series data. For example, let $x'(t) = \cos(2\pi t f)$ with $f = 96$ Hz and let $y(t_n)$ be the set of discrete samples of $x'(t)$ where the sampling scheme has the normalized spectral window function depicted in Fig. 3a. The Nyquist frequency for this sampling scheme is 100 Hz. The sidelobes centered at 2, 6, and 10 Hz in Fig. 3b are centered at 98, 104, and 106 Hz after convolving $S(f)$ with $X'(f)$. The sidelobes centered at 104 and 106 Hz are greater than the Nyquist frequency and wrap-around to 96 and 94 Hz, respectively. Notice the peak in the power spectrum corresponding to the input signal has a frequency below the Nyquist frequency and does not wrap-around but combines with the sidelobe aliased to 96 Hz. The real and imaginary components of $Y(f)$ at 96 Hz are distorted due to the aliased sidelobe.

Another property of interest is now given. Assume that $x(t)$ is the output of a constant parameter linear system. If the output of such a system is sampled unevenly, then the overall system is nonlinear. This property is demonstrated with the following example. Let $x'(t) = \cos(2\pi t f)$ with $f = 23$ Hz and let $y(t_n)$ be the set of discrete samples of $x'(t)$ where the sampling scheme has the normalized spectral window function depicted in Fig. 3a. The Fourier transform of $x'(t)$ will be zero everywhere except at $f = 23$ Hz. The Fourier transform of $Y(f)$ according to Eq. 4 is $S(f) * X'(f)$. The power spectrum of $Y(f)$ is shown in Fig. 4. In Fig. 4, the Fourier transform of $Y(f)$ is computed by convolving $S(f)$ with $X'(f)$ and by computing the Fourier transform of $y(t_n)$. The Fourier transform of $y(t_n)$ was computed using the least squares Fourier transform to eliminate error caused by numerical integration. The least squares Fourier transform is shown to be identical to the traditional Fourier transform defined in Eq. 5 in Appendix A. In Fig. 4, the two methods for computing $Y(f)$ are identical. More importantly, the sampling scheme results in the leakage of power from 23 Hz to sidelobes centered at 13, 17, 21, 25, 29, and 33 Hz. That is, a system
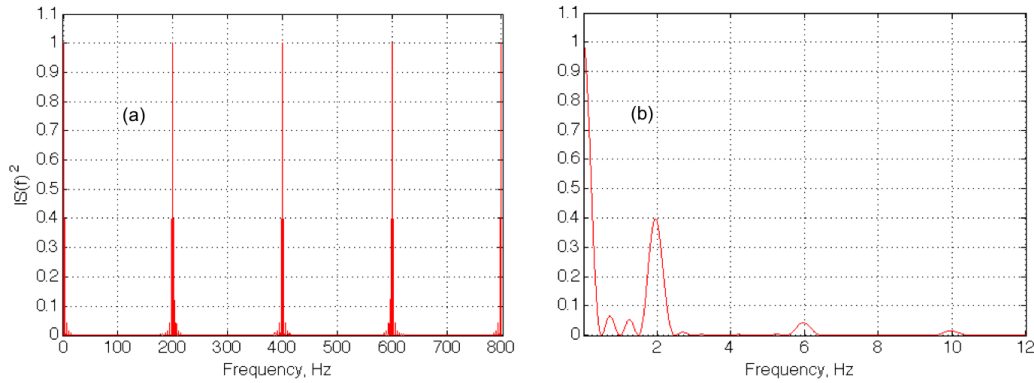
sampled unevenly causes frequency translation and is therefore nonlinear regardless of whether the transducer has a linear response.
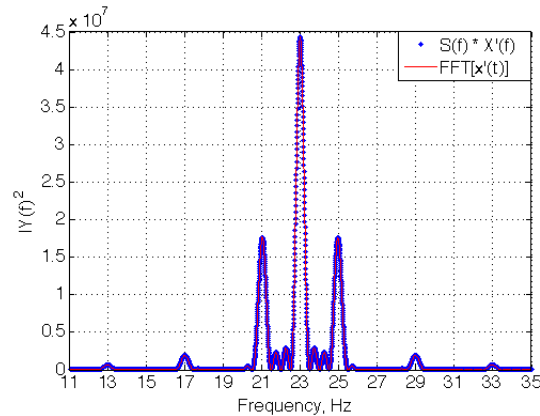
Due to the inherent nonlinearity caused by sampling unevenly, the reconstruction of $x'(t)$ from $s(t)$ and $y(t_n)$ does not in general exist. However, it has been shown that it is possible to reconstruct $x'(t)$ exactly from $s(t)$ and $y(t_n)$ if the power spectrum of $x'(t)$ is sparse, and if the frequency content of $x'(t)$ is below the Nyquist frequency evaluated at the mean sampling interval[34]. This reconstruction process requires nonlinear methods such as an iterative deconvolution and is important for the research area of compressed sensing. Unfortunately, the power spectra of surface pressure fluctuations underneath laminar, turbulent, or shock-influenced boundary layers show a continuous decrease of spectral amplitude with increasing frequency (red-noise spectrum) and hence are not sparse. Therefore, methods that estimate $x'(t)$ from $s(t)$ and/or $y(t_n)$ have to be used.

Figure 2. Power spectrum of the normalized spectral window function for an evenly sampled time series with a sample rate of 100 Hz.
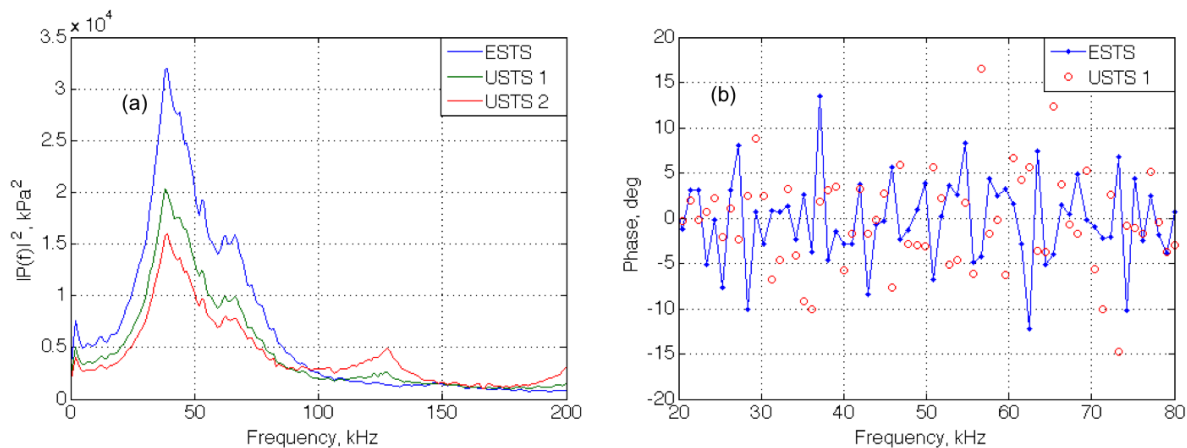

Figure 3. (a) Power spectra for the spectral window function of an unevenly sampled time series, (b) Rescaled view of Fig. 3(a) showing the sidelobes. The sampling interval was constant at 0.005 seconds with gaps between 0.250 to 0.500, 0.750 to 1.000, and 1.250 to 1.500 seconds.

Approved for public release; distribution unlimited.

Figure 4. Power spectrum computed by convolving a sinusoidal input at a single frequency of 23 Hz with the normalized spectral window function, and by computing the Fourier transform of the unevenly sampled time series.
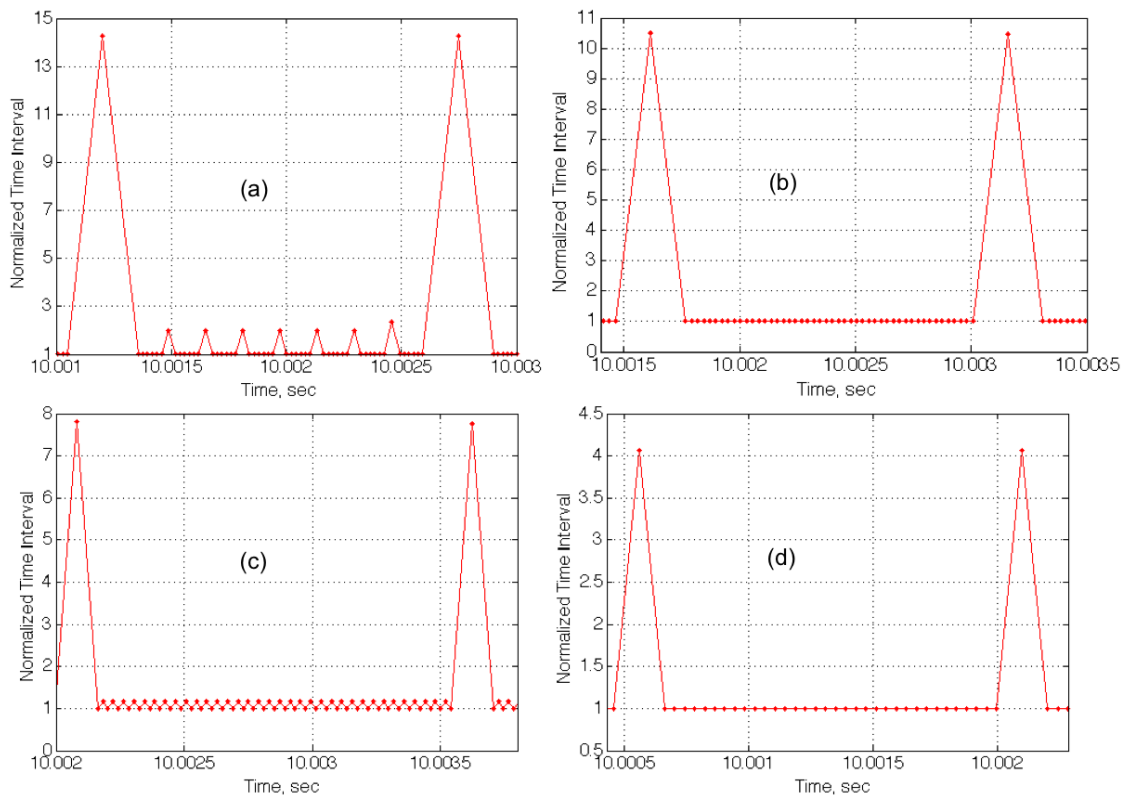
The discussion has so far focused on periodic data. The discussion is now extended to stochastic time series data such as surface pressure data recorded underneath laminar, transitional, turbulent, or shock-impinged boundary layers. The power spectra of this type of data will have nonzero power at each resolvable frequency. The frequencies with nonzero power each contribute sidelobes resulting in significant distortion of the Fourier transform due to the sum contribution of so many sidelobes. The distortion in the Fourier transform of surface pressure measurements underneath a transitional boundary layer is shown in Fig. 5. Evenly sampled surface pressure data was acquired at a sample rate of 500 kHz[35]. The corresponding Nyquist frequency was 250 kHz. Two unevenly sampled time series were generated from the evenly sampled time series by deleting every sixth and every third data point. Each time series was partitioned into 400 segments. The Fourier transform of each segment was computed using the least squares Fourier transform. The Fourier transform of each time series was determined by averaging the Fourier transform from each segment. The power spectrums of the evenly sampled and two unevenly sampled time series are shown in Fig. 5a. In Fig. 5a, the distortion caused by the sidelobes is apparent by comparing the amplitude of the evenly sampled time series (ESTS) with the amplitudes of the two unevenly sampled time series (USTS). The phase was determined for each time series by computing the arctangent of the ratio of the imaginary and real component of the Fourier transform. A comparison between the phase of the evenly sampled time series and one of the unevenly sampled time series is shown in Fig. 5b. The phase spectrum from the other unevenly sampled time series was not included for clarity purposes. In Fig. 5b, the phases of the evenly and unevenly sampled time series are different due to the distortion caused by the sidelobes.

Figure 5. (a) Power spectrum of an evenly sampled time series (ESTS), and two unevenly sampled time series generated by deleting every sixth data point (USTS 1) and every third data point (USTS 2) of the ESTS, (b) A comparison between the phase spectrum of the ESTS and USTS. The time series data correspond to surface pressure fluctuations recorded underneath a transitional boundary layer.
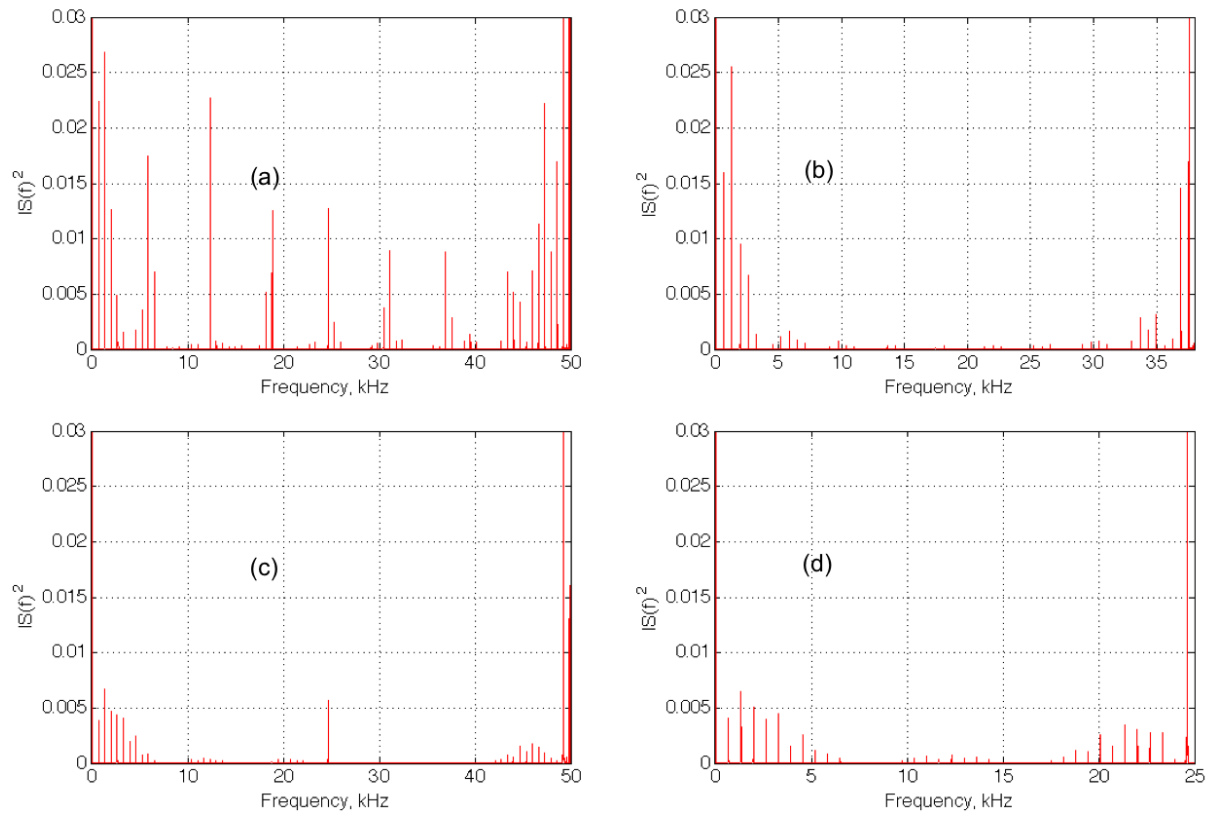
7

III.   The HIFiRE-1 Sampling Scheme

The sampling scheme for the high bandwidth pressure transducers on the cone, flare, and cylinder are shown in Figs. 6a, 6b, and 6c, respectively. In this paper, the normalized time interval is defined as $\Delta t/\min(\Delta t)$ and represents the duration between consecutive measurements in units of the time interval. As shown in Fig. 6, the sampling scheme used for each high bandwidth pressure transducer is periodic. The high bandwidth pressure transducer designated as transducer 12 was sampled at a lower rate than the rest of the transducers located on the cylinder to satisfy telemetry bandwidth constraints, as shown in Fig. 6d. As will be shown, the sample rate for transducer 12 was well below the cutoff frequency of the antialiasing filter. The sampling scheme used for the transducers distributed on the flare consisted of 48 consecutively measured data points sampled evenly for 1.2407 x 10^{-3} seconds, as shown in Fig. 6b. The fundamental frequency for these evenly sampled blocks of data is ~806 Hz and hence the frequency resolution is poor. However, the Fourier transform of these blocks of data are free of the distortion caused by sidelobes.

Figure 6. The sampling scheme for the high bandwidth pressure transducers mounted on (a) the cone, (b) the flare, (c) the cylinder (transducers 7, 8, 9, 10, 11, and 19), and (d) the cylinder (transducer 12).

The power spectrum of the normalized spectral window functions for the high bandwidth pressure transducers mounted on the cone, flare, and cylinder are shown in Figs. 7a, 7b, and 7c, respectively. The power spectrum of the normalized spectral window function is riddled with many sidelobes. As demonstrated in the previous section, these sidelobes cause significant distortion of the Fourier transform. The mean Nyquist frequency, computed using the mean sampling interval and Eq. 1, are given as 17.81, 15.87, and 22.67 kHz for the transducers mounted on the cone, flare, and cylinder, respectively. The cone transducers were bandpass-filtered at 100 Hz – 30 kHz, and those on the cylinder and flare were filtered at 100 Hz – 20 kHz. Signals on the cone and flare were thus subject to some aliasing at higher frequencies, but the cylinder transducers should be free of aliasing.

Approved for public release; distribution unlimited.

Figure 7. Power spectrum of the spectral window function for the high bandwidth pressure transducers mounted on (a) the cone, (b) the flare, (c) the cylinder (transducers 7, 8, 9, 10, 11, and 19), and (d) the cylinder (transducer 12).

IV.   Linear Interpolation

Resampling irregularly spaced data onto a uniformly spaced grid by interpolation eliminates the nonlinear sidelobes, as can be shown by computing the spectral window function. However, interpolation acts as a low-pass filter, significantly reducing the power of the higher resolvable frequencies of the data. The amount of power loss depends on the interpolation scheme. In general, every interpolation scheme acts as a low-pass filter causing some power loss[36].

The grid spacing for an evenly spaced grid, which is commonly referred to as the resampling time, is given as

$$t_r = \frac{1}{2 f_c} \tag{6}$$

where the Nyquist frequency is determined from the period of the spectral window function. The uniform grid is given as $t_n = t_0 + (n-1)t_r$ for $n = 1, 2, 3 \ldots (t_f - t_0)/t_r$ where t_0 and t_f are the initial and final times of the time series.

The discussion will now focus on estimating the power loss caused by resampling the HIFiRE-1 data onto a grid with grid spacing t_r. The objective will be to determine a time-series with analytically described spectral characteristics similar to the expected HIFiRE-1 pressure signals. The spectral distortion caused by uneven sampling can then be quantified, and this known distortion can then be used to determine the transfer function of the resampling process.

Consider Langevin's equation describing the velocity $x(t_n)$ of a Brownian particle given as

9

Approved for public release; distribution unlimited.

$$dx(t) = \tau x(t)dt + d\xi(t) \tag{7}$$

where $\tau < 0$ and $\xi(t)$ represents a random process consistent with Brownian motion. According to Robinson[37], the velocity samples generated by Eq. 7 are also generated by

$$x(t_n) = \exp\left(-\frac{t_n - t_{n-1}}{\tau}\right)x(t_{n-1}) + \varepsilon(t_n) \tag{8}$$

where

$$\varepsilon(t_n) \sim N\left\{0, 1 - \exp\left(-2\frac{t_n - t_{n-1}}{\tau}\right)\right\}. \tag{9}$$

In Eq. 9, ε represents the random component of the time series and is assumed to have a normal distribution with a mean and variance of zero and $1 - \exp\left(-2\frac{t_n - t_{n-1}}{\tau}\right)$, respectively. The autospectral density function can be determined by computing the Fourier transform of the autocorrelation function of Eq. 8 and is given as

$$G_{\tilde{x}\tilde{x}}(f) = G_0 \frac{1 - \rho^2}{1 - 2\rho\cos\left(\frac{\pi f}{f_c}\right) + \rho^2} \tag{10}$$

where G_0 is the average spectral amplitude and ρ is given as

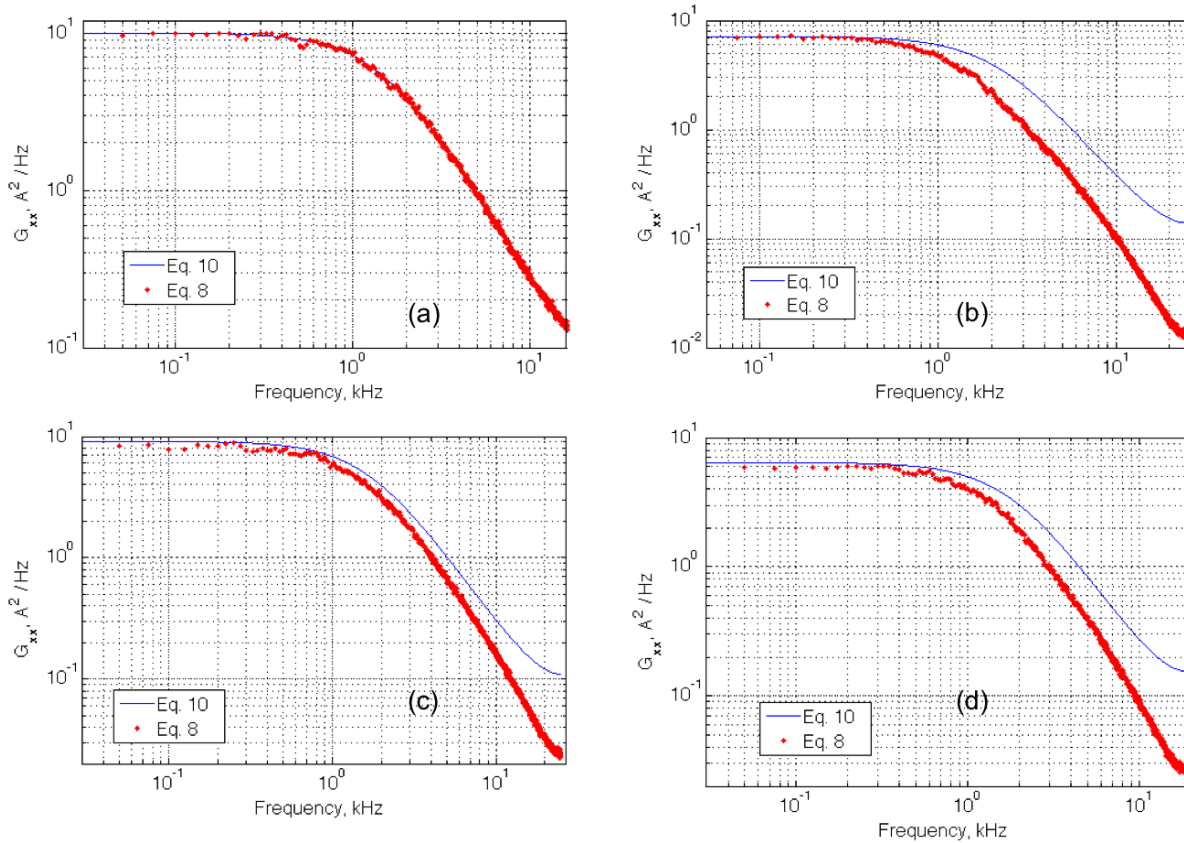$$\rho = \exp\left(-\frac{\overline{\Delta t}}{\tau}\right). \tag{11}$$

In Eq. 11, τ is a time constant and represents the decay period of the autocorrelation function, and $\overline{\Delta t}$ is the average sampling interval given as

$$\overline{\Delta t} = \frac{t_N - t_1}{N - 1}. \tag{12}$$

According to Robinson[37], Eq. 8 may be thought of as a first order autoregressive model with time-varying coefficients and heteroscedastic errors.

Equations 8 and 10 provide a way to compute time series data with a known autospectral density function for any arbitrary sampling scheme. Equations 8 through 12 were validated by generating time series data for uniformly spaced samples and then comparing the autospectral density functions computed using Eq. 10 and computed directly from the time series data using the procedures given in Bendat and Piersol[38]. The comparison is nearly identical, as shown in Fig. 8a.

The power loss caused by resampling the HIFiRE-1 data was estimated by generating time series data using Eq. 8 for the HIFiRE-1 sampling scheme. This time series was interpolated onto an evenly spaced grid. The autospectral density function was determined directly from Eq. 10 and compared with the autospectral density function computed from the interpolated time series. Comparisons are shown in Figs. 8b, 8c, and 8d for the sampling schemes used by the pressure transducers located on the cone, flare, and cylinder, respectively. The results shown in Figs. 8b, 8c, and 8d are for a linear interpolation scheme. Other interpolation methods were investigated and yielded similar results. As shown in the Fig. 8, the power loss was greatest for the transducers located on the cone, whereas, the transducers located on the flare experienced the least power loss. It is reasonable that the transducers on the cone experienced a greater power reduction than the transducers on the flare because the data collected on the cone were missing more samples than the data collected on the flare, as shown in Fig. 6. Similarly, blocks of data riddled with many missing data points such as near the beginning of the first and second stage rocket burn will experience the most power reduction. The uncertainty for these blocks of data will be greater than blocks of data with fewer missing samples.

Approved for public release; distribution unlimited.

Figure 8. (a) Equation 8 and Eq. 10 are compared for a uniformly spaced sampling scheme, (b) The sampling scheme of the pressure transducers located on the cone are used to generate a time series with Eq. 8. The time series is interpolated and the autospectral density function is computed and compared to the theoretical autospectral density function, (c) The theoretical autospectral density function is compared to the autospectral density function computed from interpolated data for the sampling scheme used by the transducers mounted on the flare, (d) The theoretical autospectral density function is compared to the autospectral density function computed from interpolated data for the sampling scheme used by the transducers mounted on the cylinder.

V.   Compensation Method for Estimating the Autospectral Density Function

As discussed in the previous section, interpolating unevenly sampled data onto an evenly spaced grid eliminates the nonlinear sidelobes but acts as a low-pass filter reducing the power of the higher frequency content of the time series data. In this section, a method is developed to compensate the reduction in power caused by linear interpolation. The compensation method developed in this section is very similar to the method given by Schulz and Mudelsee[39]. After compensation, the autospectral density function is similar to the autospectral density function of $x'(t)$.

It is assumed that the time series data does not have sinusoidal periodic, complex periodic, or almost-periodic components and is a stochastic time series with a red-noise "like" autospectral density function. Sinusoidal components should be removed from the time series before compensation. The steps for the compensation method are as follows:

1. Determine τ by fitting the measured data with Eq. 8. There are two equivalent approaches for determining τ in Eq. 8 from the measured data. The first approach is to use the estimation procedure given by Mudelsee[40], which utilizes Brent's method. The second approach consists of more steps but utilizes the equations given in this paper. To begin, interpolate the measured data onto a uniformly spaced grid and determine the autoregressive coefficient given as

Approved for public release; distribution unlimited.

$$\hat{\varphi}_1 = \exp\left(-\frac{\Delta t}{\tau}\right) \tag{13}$$

by fitting the interpolated data using least squares given as

$$\begin{bmatrix} \sum_{m=n+1}^{M} x_{m-1}^2 & \sum_{m=n+1}^{M} x_{m-1}x_{m-2} \\ \sum_{m=n+1}^{M} x_{m-1}x_{m-2} & \sum_{m=n+1}^{M} x_{m-2}^2 \end{bmatrix} \begin{bmatrix} \hat{\varphi}_0 \\ \hat{\varphi}_1 \end{bmatrix} = \begin{bmatrix} \sum_{m=n+1}^{M} x_m x_{m-1} \\ \sum_{m=n+1}^{M} x_m x_{m-2} \end{bmatrix}. \tag{14}$$

In Eq. 14, M is the total number of autoregressive coefficients. The time constant is given as

$$\tau_{fit} = -\frac{\Delta t}{\log \hat{\varphi}_1}. \tag{15}$$

The time constant given in Eq. 15 does not actually correspond to τ of the measured data. Instead, an iterative procedure is required to determine the appropriate value for τ. To do so, τ is assigned an initial value designated as τ'. Next, compute a time series using Eq. 8 for the same sampling scheme as the measured data for $\tau = \tau'$. Interpolate this time series onto the same uniformly spaced grid as the measured time series data. Determine the time constant designated as $\tilde{\tau}$ for this time series using Eqs. 14 and 15. Adjust τ' so that $|\tilde{\tau} - \tau_{fit}| \to 0$. The time constant of the measured data is then estimated as τ'.

2. Compute an autoregressive time series using Eq. 8 for $\tau = \tau'$.

3. Interpolate the time series data from Step 2 and compute the autospectral density function. The autospectral density function from this step is designated as G'_{AR}.

4. Compute the autospectral density function of the time series data from Step 2 using Eq. 10. The autospectral density function from this step is designated as G_{AR}.

5. Compute the compensation factor given as
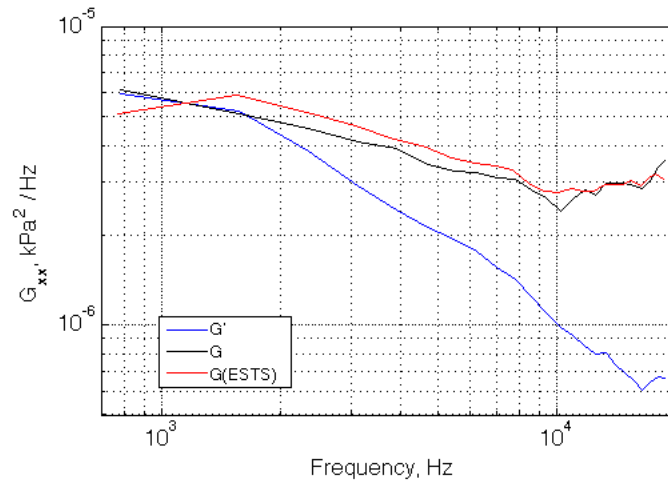
$$H(f) = \frac{G_{AR}(f)}{G'_{AR}(f)}. \tag{16}$$

6. Determine the compensated autospectral density function given as

$$G_{xx}(f) = H(f)G'_{xx}(f) \tag{17}$$

where $G'_{xx}(f)$ is the autospectral density function of the measured data interpolated onto an evenly spaced grid.
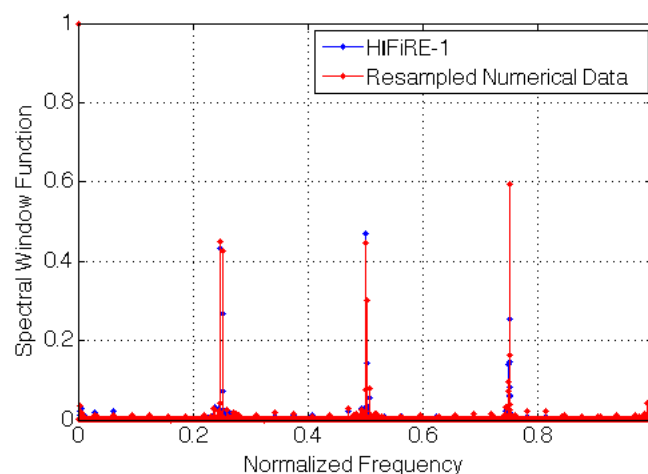
The compensation method was checked in two ways. In one approach, short blocks of flight data with even sampling rates provided spectra undistorted by uneven sampling time intervals. In the second approach, a large-eddy simulation (LES) of a turbulent shock boundary-layer interaction provided a time-series that could be evenly and unevenly sampled. The evenly-sampled LES time series provided a truth-model against which to compare the unevenly-sampled, compensated spectrum.

As shown in Fig. 6b, the flight sampling scheme on the flare featured evenly sampled blocks of data separated by gaps with duration of approximately 10.5 sampling intervals. The autospectrum was determined by averaging the autospectrum computed for 1200 evenly sampled blocks of data. This spectrum is treated as a known spectrum with frequency resolution of approximately 800 Hz. This known spectrum is designated as $G(ESTS)$. The autospectrum of unevenly sampled data was determined from the flare data by partitioning the data into blocks with the gaps. As shown in Fig. 9, $G'_{xx}(f)$ is significantly lower than $G(ESTS)$ for frequencies greater than 2 kHz. A comparison between $G_{xx}(f)$ and $G(ESTS)$ shows that the compensation method recovers the correct roll off and power levels.
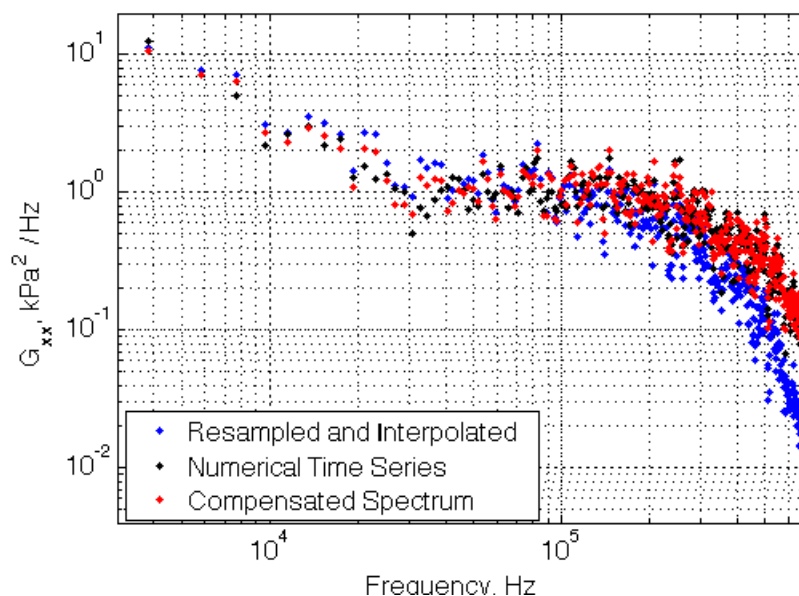
12

Figure 9. Comparison between $G'_{xx}(f)$ and $G_{xx}(f)$ with a baseline spectrum, designated as $G(ESTS)$ for surface pressure measurements recorded by transducer 21 located on the flare. The baseline spectrum was determined from the evenly sampled blocks of data shown in Fig. 6b.

The compensation method was also validated using numerical time series data.[41] This numerical time series was sampled evenly at a sample rate of 192.9 MHz. The numerical time series was resampled to match the sampling scheme used for the transducers located on the cone. The numerical time series was digitally low-pass filtered prior to resampling in the same pass-band as the HIFiRE-1 data. Resampling was accomplished by sampling the time series using the sampling scheme shown in Fig. 6a. Since the numerical time-series was sampled at discrete time intervals, the uneven sampling rate was similar to the HIFiRE sampling rate, but did not exactly reproduce it. The spectral window functions for the sampling scheme of the cone transducers and the resampled numerical time series are shown in Fig. 10. As shown, the spectral window functions are very similar, thus the distortion caused by sidelobes in the autospectral density function should be very similar for the two time series. In Fig. 11, the autospectral density function was determined for the evenly spaced numerical time series, the unevenly spaced numerical time series interpolated onto an evenly spaced grid, and the unevenly-spaced time series, interpolated and compensated. As shown in Fig. 11, the compensation method recovers the roll-off and power loss caused by interpolating the unevenly sampled numerical time series onto an evenly spaced grid. This numerical experiment and the comparison of unevenly to evenly-spaced flight data confirm the validity of the compensation method.

Figure 10. Comparison between the spectral window functions of the sampling scheme used in flight by the transducers located on the cone with the resampled numerical time series. The frequencies were normalized by the Nyquist frequency of each sampling scheme.

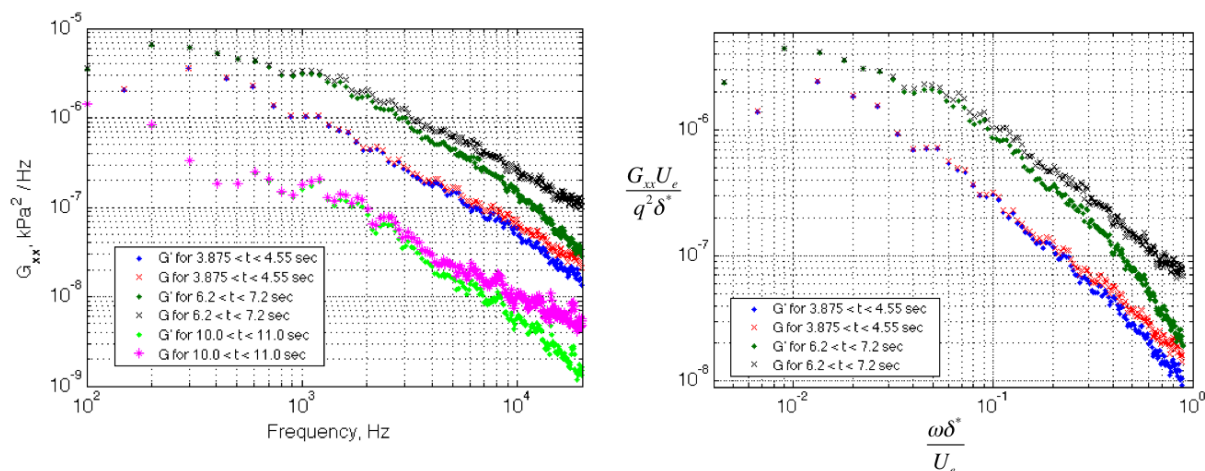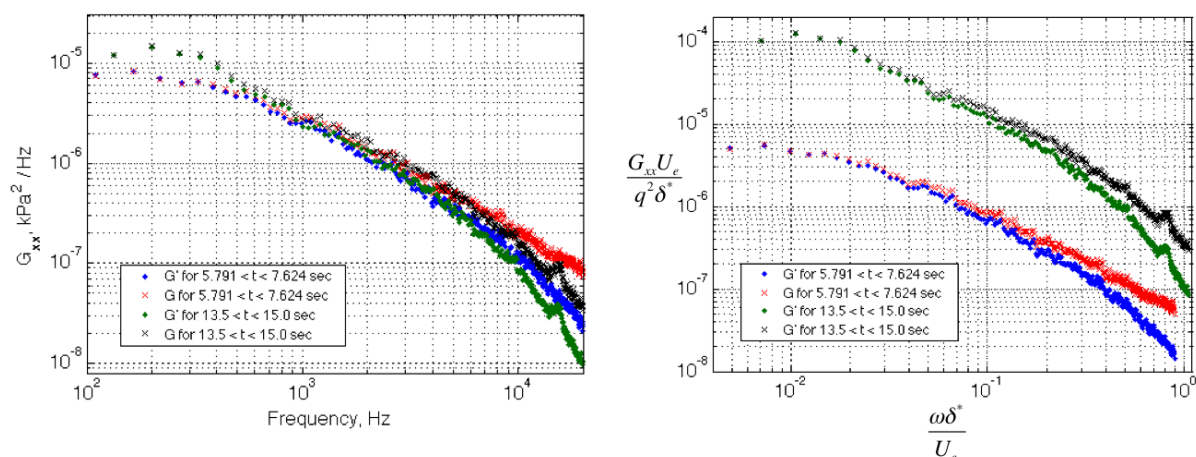Approved for public release; distribution unlimited.

Figure 11. Comparison between the autospectral density function of the compensated spectrum, the evenly sampled numerical time series, and the resampled numerical time series interpolated onto an evenly spaced grid.

A comparison between the dimensional and nondimensional $G'_{xx}(f)$ and $G_{xx}(f)$ for surface pressure measurements recorded at different times during the ascent by transducers 7 and 9 located on the cylinder are shown in Figs. 12 and 13. These transducers were located respectively 8 and 6 cm upstream of the flare. The frequency and autospectral density function were normalized using the 99 percent boundary-layer thickness, and the dynamic pressure. These normalizing quantities were provided by Robert Yentsch of The Ohio State University. The flight conditions for the times shown in Figs. 12 and 13 are summarized in the table below. Times prior to t=6 seconds correspond to the first-stage boost phase. Times between t=6 and t=15 seconds correspond to the coast phase between first-stage burnout and second-stage ignition.

The flight data show a rolloff in amplitude with increasing frequency, typical of that seen in shock-boundary interactions.[42] As shown in the figure, the compensation method does not noticeably alter power levels for frequencies below 1.5 – 3 kHz but becomes more prominent as the frequency increases. The compensated spectra roll off at a rate of about 8 dB/octave. This rolloff rate is slightly lower than that observed in Ref 41, but similar to other data cited in the same reference. These data, combined with checks against numerical experiment and small blocks of evenly-sampled flight data, indicate that unevenly-sampled flight data may be analyzed to provide meaningful spectral data.

14

Approved for public release; distribution unlimited.

Figure 12. (a) Comparison between $G'_{xx}(f)$ and $G_{xx}(f)$ determined from surface pressure measurements recorded at different times during the ascent, (b) Comparison between normalized $G'_{xx}(f)$ and $G_{xx}(f)$ versus normalized frequency.

Figure 13. (a) Comparison between $G'_{xx}(f)$ and $G_{xx}(f)$ determined from surface pressure measurements recorded at different times during the ascent, (b) Comparison between normalized $G'_{xx}(f)$ and $G_{xx}(f)$ versus normalized frequency.

Table – Flight Conditions Analyzed

Approved for public release; distribution unlimited.

Time, sec	Freestream Mach, M	Freestream Unit Reynolds Number per meter
3.870	2.14	4.26E+07
4.550	2.61	4.95E+07
6.200	3.43	5.57E+07
7.200	3.25	4.71E+07
5.791	3.41	5.80E+07
7.624	3.19	4.44E+07
10.000	2.90	3.20E+07
11.000	2.83	2.88E+07
13.500	2.67	2.21E+07
15.000	2.58	1.89E+07

VI.   Conclusion

Computing the autospectral density function directly from an unevenly sampled time series results in a distorted spectrum. The distortion is caused by nonlinear sidelobes that are nonzero only for unevenly sampled data. This nonlinearity can be removed by resampling the unevenly sampled time series onto an evenly spaced grid at the cost of under predicting the power of the higher frequency components of the time series data. A compensation method was implemented to recover the power lost by resampling. Specifically, the compensation method developed in this paper estimates the autospectral density function of stochastic, surface pressure data having red-noise "like" spectra sampled unevenly during the HIFiRE-1 flight experiment. This compensation method estimates the autospectral density function by determining a correction factor. The coefficients of a first order autoregressive model, that holds for unevenly sampled data, are determined from the measured time series data using a nonlinear least squares procedure. The autoregressive coefficients are used to generate a time series with the same sampling scheme as the surface pressure data. This autoregressive time series and measured time series are resampled onto an evenly spaced grid. The autospectral density function is computed from the resampled autoregressive time series, the resampled measured data, and directly from the autoregressive coefficients. A correction factor is determined by taking the ratio of the autospectral density function computed from the autoregressive coefficients with the autospectral density function of the resampled autoregressive time series. The autospectral density function of the measured data is estimated by multiplying the correction factor with the autospectral density function of the resampled measured pressure data.

The time series data measured during the flight experiment has some aerothermal data that would benefit from correlation-based analysis such as crossflow instabilities, rolling and pitching motions of the payload, and shock-foot motion overtop surface mounted transducers. Future work will investigate methods for preserving the phase information of the time series data recorded during the HIFiRE-1 flight.

Acknowledgments

Approved for public release; distribution unlimited.

References

[1]Dolvin, D. J., "Hypersonic Flight Research and Experimentation (HIFiRE) Fundamental Sciences and Technology Development Strategy," AIAA paper 2008-2581, 2008.

[2]Dolvin, D. J., "Hypersonic International Flight Research and Experimentation Technology Development and Flight Certification Strategy," AIAA paper 2009-7228, 2009.

[3]Kimmel, R. L., Adamczak, D. and DSTO AVD Brisbane Team, "HIFiRE-1 Preliminary Aerothermodynamic Measurements," AIAA paper 2011-3413, 2011.

[4]Kimmel, R. L., Adamczak, D., Gaitonde, D., Rougeux, A. and Hayes, J. R., "HIFiRE-1 Boundary Layer Transition Experiment Design," AIAA paper 2007-534, 2007.

[5]Wadhams, T. P., MacLean, M. G., Holden, M. S. and Mundy E., "Pre-Flight Ground Testing of the Full Scale Fresh FX-1at Fully Duplicated Flight Conditions," AIAA paper 2007-4488, 2007.

[6]Johnson, H. B., Alba, C. R., Candler, G. V., MacLean, M., Wadhams, T. and Holden, M., "Boundary-Layer Stability Analysis of the Hypersonic International Flight Research Transition Experiments," *Journal of Spacecraft and Rockets*, vol. 45, pp. 228-236, 2008.

[7]Kimmel, R. L., "Aerothermal Design for the HIFiRE-1 Flight Vehicle," AIAA paper 2008-4034, 2008.

[8]Casper, K. M., Wheaton, B. M., Johnson, H. B. and Schneider, S. P., "Effect of Freestream Noise on Roughness-Induced Transition at Mach 6," AIAA paper 2008-4291, 2008.

[9]Kimmel, R. L., "Roughness Considerations for the HIFiRE-1 Vehicle," AIAA paper 2008-4293, 2008.

[10]Alba, C. R., Johnson, H. B., Bartkowicz, M. D., Candler, G. V. and Berger, K. T., "Boundary-Layer Stability Calculations for the HIFiRE-1 Transition Experiment," *Journal of Spacecraft and Rockets*, vol. 45, pp. 1125-1133, 2008.

[11]Wadhams, T. P., Mundy, E., MacLean, M. G. and Holden, M. S., "Ground Test Studies of the HIFiRE-1 Transition Experiments Part 1: Experimental Results," *Journal of Spacecraft and Rockets*, vol. 45, pp. 1134-1148, 2008.

[12]MacLean, M., Wadhams, T., Holden, M. and Johnson, H., "Ground Test Studies of the HIFiRE-1 Transition Experiment Part 2: Computational Analysis," *Journal of Spacecraft and Rockets*, vol. 45, pp. 1149-1164, 2008.

[13]Berger, K. T., Greene, F. A., Kimmel, R, L., Alba, C. and Johnson, H., "Aerothermodynamic Testing and Boundary-Layer Trip Sizing of the HIFiRE Flight 1 Vehicle," *Journal of Spacecraft and Rockets*, vol. 46, pp. 473-480, 2009.

[14]Adamczak, D., Alesi, H. and Frost, M., "HIFiRE-1: Payload Design, Manufacture, Ground Test, and Lessons Learned," AIAA paper 2009-7294, 2009.

[15]Gaitonde, D. V., Kimmel, R. L., Jackson, D. and Zhong, X., "CFD Analysis in Development of Flight Test Article for Basic Research," AIAA paper 2006-8085, 2006.

[16]Babu, P. and Stoica, P., "Spectral Analysis of Nonuniformly Sampled Data – A Review," *Digital Signal Processing*, Vol. 20, pp. 359-378, 2010.

[17]Barning, F. J. M., "The Numerical Analysis of the Light-Curve of 12 Lacertae," *Bull. Astron. Inst. Neth.,* Vol. 17, No. 1, pp. 22-28, 1963.

[18]Lomb, N. R., "Least-Squares Frequency Analysis of Unequally Spaced Data," *Astrophysics and Space Sciences*, Vol. 39, pp. 447-462, 1976.

[19]Scargle, J. D., "Studies in Astronomical Time Series Analysis. II. Statistical Aspects of Spectral Analysis of Unevenly Spaced Data," *The Astrophysical Journal*, Vol. 263, pp. 835-853, 1982.

[20]Scargle, J. D, "Studies in Astronomical Time Series Analysis. III. Fourier Transforms, Autocorrelation Functions, and Cross-Correlation Functions of Unevenly Spaced Data," *The Astrophysical Journal*, Vol. 343, pp. 874-887, 1989.

[21]Schulz, M. and Stattegger, K., "Spectrum: Spectral Analysis of Unevenly Spaced Paleoclimatic Time Series," *Computers & Geosciences*, Vol. 23, pp. 929-945, 1997.

[22]Stoica, P., Li, J., and He, H., "Spectral Analysis of Nonuniformly Sampled Data: A New Approach Versus the Periodogram," *IEEE Trans. Signal Process.*, Vol. 57, pp. 843-858, 2009.

[23]Horowitz, L. L., "The Effects of Spline Interpolation on Power Spectral Density," *IEEE Trans. Audio Electroacoust.*, Vol. ASSP-22, pp. 22-27, 1974.

[24]Tropea, C., "Laser Doppler Anemometry: Recent Developments and Future Challenges," *Meas. Sci. Technol.*, Vol. 6, pp. 605-619, 1995.

[25]Mayo, W. T., Shay, M. T., and Riter, S., "Digital Estimation of Turbulence Power Spectra from Burst Counter LDV," *2nd International Workshop on Laser Velocimetry Proceedings*, Vol. 1, AF-10426-01-35, pp. 16-24, 1974.

Approved for public release; distribution unlimited.

[26]Larsson, E. K., "Identification of Stochastic Continuous-Time Systems," *PhD. Thesis*, Uppsala University, 2004.

[27]Martin, R. J., "Irregularly Sampled Signals: Theories and Techniques for Analysis," *PhD. Thesis*, University College London, 1998.

[28]Baisch, S. and Bokelmann, G. H. R., "Spectral Analysis with Incomplete Time Series: An Example from Seismology," *Computers & Geosciences*, Vol. 25, pp. 739-750, 1999.

[29]Fortin, P and Mackey, M., "Periodic Chronic Myelogenous Leukaemia: Spectral Analysis of Blood Cell Counts and Aetiological Implications," *British Journal of Haematology*, Vol. 104, pp. 336-345, 1999.

[30]Li, L., Li, K., Liu, C., and Liu, C., "Comparison of Detrending Methods in Spectral Analysis of Heart Rate Variability," *Research Journal of Applied Physics, Engineering, and Technology,* Vol. 3, pp. 1014-1021, 2011.

[31]Zhao, W., Serpedin, E. and Dougherty, E. R., "Spectral Preprocessing for Clustering Time-Series Gene Expressions," *EURASIP Journal on Bioinformatics and System Biology*, Article ID 713248, 2009.

[32]Deeming, T. J., "Fourier Analysis with Unequally-Spaced Data," *Astrophysics and Space Science*, Vol. 36, pp. 137-158, 1975.

[33]Eyer, L. and Bartholdi, P., "Variable Stars: which Nyquist Frequency," *Astronomy and Astrophysics*, Vol. 135, pp. 1-3, 1999.

[34]Marks, R. J., *Advanced Topics in Shannon Sampling and Interpolation Theory*, Springer-Verlag, New York, 1993, Chap. 4.

[35]Borg, M., Kimmel, R., and Stanfield, S., "HIFiRE-5 Attachment-Line and Crossflow Instability in a Quiet Hypersonic Wind Tunnel," AIAA paper 2011-3247, 2011.

[36]Müller, E., Nobach, H., and Tropea, C., "LDA Signal Reconstruction: Application to Moment and Spectral Estimation," *7th Int. Symp. On Applications of Laser Technology to Fluid Mechanics*, 1994.

[37]Robinson, P. M., "Estimation of a Time Series Model from Unequally Spaced Data," *Stochastic Processes and their Applications*, Vol. 6, pp. 9-24, 1977.

[38]Bendat, J. S., and Piersol, A. G., *Random Data Analysis and Measurement Procedures, 4th Ed.,* John Wiley & Sons, Inc., New Jersey, 2010, pp. 386 – 404.

[39]Schulz, M, and Mudelsee, M., "REDFIT: Estimating Red-Noise Spectra Directly from Unevenly Spaced Paleoclimatic Time series," *Computers & Geosciences*, Vol. 28, pp. 421-426, 2002.

[40]Mudelsee, M., "TAUEST: A Computer Program for Estimating Persistence in Unevenly Spaced Weather / Climate Time Series," *Computers & Geosciences*, Vol. 28, pp. 69-72, 2002.

[41]Poggie, J., Bisek, N. J., Kimmel, R. L., Stanfield, S. A., "Spectral Characteristics and Reduced-Order Modeling of Separation Shock Unsteadiness," AIAA paper, 43rd AIAA Fluid Dynamics Conference, June 2013.

[42]Dolling, D. S. and Or, C. T., "Unsteadiness of the Shock Wave Structure in Attached and Separated Compression Ramp Flows," *Experiments in Fluids*, Vol. 3, 1985, pp. 24-32.

Appendix A: Least Squares Fourier Transform

In this section, the least squares periodogram and the least squares Fourier transform are developed quantitatively by summarizing the results given in References 17-21. The discrete Fourier transform is defined as

$$FT(\omega) = \sum_{n=1}^{N} y_n \exp(-i\omega t_n) \tag{A1}$$

where ω is the angular frequency given as $\omega = 2\pi f$. The classical periodogram is defined as

$$P_x(\omega) = \frac{1}{N}|FT(\omega)|^2. \tag{A2}$$

Substituting Eq. A1 into Eq. A2 gives

$$P_x(\omega) = \frac{1}{N}|\sum_{n=1}^{N} y_n \exp(-i\omega t_n)|^2 \tag{A3}$$

or

$$P_x(\omega) = \frac{1}{N}\{[\sum_{n=1}^{N} y_n \cos(\omega t_n)]^2 + [\sum_{n=1}^{N} y_n \sin(\omega t_n)]^2\}. \tag{A4}$$

18
Approved for public release; distribution unlimited.

In the derivation that follows, the time series data $y(t)$ is fit with the model $a_j \cos(\omega_j t_n) + b_j \sin(\omega_j t_n)$ using the method of least squares. The derived least squares fit is then shown to be equivalent to the classical periodogram defined in Eq. A4. The equivalence includes the preservation of the statistical properties of the classical periodogram. The least squares Fourier transform is then defined using the least squares periodogram.

The sum of squares is given as

$$R = \sum_{n=1}^{N}\{y_n - [a_j \cos(\omega_j t_n) + b_j \sin(\omega_j t_n)]\}^2 \tag{A5}$$

For a simultaneous reduction of $\omega = \omega_1, \omega_2, \dots \omega_j$, the corresponding parameters a_j and b_j are chosen such that the stationary conditions $\frac{\partial R}{\partial a_j} = \frac{\partial R}{\partial b_j} = 0$. The stationary conditions are given as

$$\frac{\partial R}{\partial a_j} = \sum_{n=1}^{N}\{y_n \cos(\omega_j t_n) - a_j \cos^2(\omega_j t_n) - b_j \sin(\omega_j t_n) \cos(\omega_j t_n)\} = 0 \tag{A6}$$

$$\frac{\partial R}{\partial b_j} = \sum_{n=1}^{N}\{y_n \sin(\omega_j t_n) - a_j \cos(\omega_j t_n) \sin(\omega_j t_n) - b_j \sin^2(\omega_j t_n)\} = 0 \tag{A7}$$

Adopting the notation

$$CC = \sum_{n=1}^{N} \cos^2(\omega_j t_n), \tag{A8}$$

$$SS = \sum_{n=1}^{N} \sin^2(\omega_j t_n), \tag{A9}$$

$$CS = \sum_{n=1}^{N} \cos(\omega_j t_n) \sin(\omega_j t_n), \tag{A10}$$

$$YC = \sum_{n=1}^{N} y_n \cos(\omega_j t_n), \tag{A11}$$

and

$$YS = \sum_{n=1}^{N} y_n \sin(\omega_j t_n), \tag{A12}$$

the stationary conditions reduce to

$$\frac{\partial R}{\partial a_j} = YC - a_j CC - b_j CS = 0 \tag{A13}$$

and

$$\frac{\partial R}{\partial b_j} = YS - a_j CS - b_j SS = 0. \tag{A14}$$

Rearranging Eq. A13 and A14 gives

$$YC = a_j CC + b_j CS = 0, \tag{A15}$$

$$YS = a_j CS + b_j SS = 0, \tag{A16}$$

or

$$\begin{bmatrix} YC \\ YS \end{bmatrix} = \begin{bmatrix} CC & CS \\ CS & SS \end{bmatrix} \begin{bmatrix} a_j \\ b_j \end{bmatrix}. \tag{A17}$$

The two equations represented in Eq. A17 are the so-called normal equations for least squares. Solving Eq. A17 for the a_j and b_j coefficients gives

19

Approved for public release; distribution unlimited.

$$\begin{bmatrix} a_j \\ b_j \end{bmatrix} = \begin{bmatrix} CC & CS \\ CS & SS \end{bmatrix}^{-1} \begin{bmatrix} YC \\ YS \end{bmatrix} = \frac{1}{CC \cdot SS - CS^2} \begin{bmatrix} SS & -CS \\ -CS & CC \end{bmatrix} \begin{bmatrix} YC \\ YS \end{bmatrix}. \tag{A18}$$

From Eq. A5 and A18, the sum of squares becomes

$$\Delta R = R - \sum_{n=1}^{N} y_n^2 = \frac{[YC \quad YS]}{CC \cdot SS - CS^2} \begin{bmatrix} SS & -CS \\ -CS & CC \end{bmatrix} \begin{bmatrix} YC \\ YS \end{bmatrix}. \tag{A19}$$

At this point ΔR is not yet in the form of the classical periodogram. In order to show equivalence between the least squares periodogram and the classical periodogram, the model $a_j \cos(\omega_j t_n) + b_j \sin(\omega_j t_n)$ is replaced by $a_j \cos[\omega_j(t_n - \tau)] + b_j \sin[\omega_j(t_n - \tau)]$ where τ is defined so that $CS = 0$ for each t_n. Solving $CS = \sum_{n=1}^{N} \cos(\omega_j t_n) \sin(\omega_j t_n) = 0$ for τ gives

$$\tau = \frac{1}{2\omega_j} \tan^{-1} \left[\frac{\sum_{n=1}^{N} \sin(2\omega_j t_n)}{\sum_{n=1}^{N} \cos(2\omega_j t_n)} \right]. \tag{A20}$$

Equations A18 and A19 become

$$\begin{bmatrix} a_j \\ b_j \end{bmatrix} = \begin{bmatrix} CC & 0 \\ 0 & SS \end{bmatrix}^{-1} \begin{bmatrix} YC \\ YS \end{bmatrix} = \begin{bmatrix} 1/CC & 0 \\ 0 & 1/SS \end{bmatrix} \begin{bmatrix} YC \\ YS \end{bmatrix} \tag{A21}$$

and

$$\Delta R = [YC \quad YS] \begin{bmatrix} 1/CC & 0 \\ 0 & 1/SS \end{bmatrix} \begin{bmatrix} YC \\ YS \end{bmatrix} \tag{A22}$$

or

$$\Delta R = \frac{YC^2}{CC} + \frac{YS^2}{SS} = \left(\frac{YC}{\sqrt{CC}} \right)^2 + \left(\frac{YS}{\sqrt{SS}} \right)^2. \tag{A23}$$

By assuming that CC and $SS \cong N/2$, Eq. A23 becomes

$$\Delta R \approx \left(\sqrt{\frac{2}{N}} YC \right)^2 + \left(\sqrt{\frac{2}{N}} YS \right)^2, \tag{A24}$$

$$\Delta R \approx \frac{2}{N} (YC)^2 + \frac{2}{N} (YS)^2, \tag{A25}$$

and

$$\Delta R \approx \frac{2}{N} \left[\sum_{n=1}^{N} y_n \cos(\omega_j t_n) \right]^2 + \frac{2}{N} \left[\sum_{n=1}^{N} y_n \sin(\omega_j t_n) \right]^2. \tag{A26}$$

By comparing Eqs. A26 and A4, it is concluded that the least squares periodogram is equivalent to the classical periodogram.

   While the definition of τ in Eq. A20 conveniently reduces the normal equations, establishing equivalence between the least squares and classical periodogram, it also preserves the time invariance property. This can easily be demonstrated by translating t_n by T_0, given as $t_n + T_0$. Under this translation, τ becomes $\tau + T_0$ and $\omega_j(t_n - \tau)$ becomes $\omega_j(t_n + T_0 - \tau - T_0)$, which is $\omega_j(t_n - \tau)$. By maintaining time invariance, the statistical properties of the classical periodogram are identical to the statistical properties of the least squares periodogram.

   With the least squares periodogram defined as

Approved for public release; distribution unlimited.

$$P_{LS}(\omega_j) = \left(\frac{YC}{\sqrt{CC}}\right)^2 + \left(\frac{YS}{\sqrt{SS}}\right)^2, \tag{A27}$$

it is now advantageous to redefine the Fourier transform. By comparing Eqs. A2 and A27, the magnitudes of the real and imaginary components of the Fourier transform are given as $\frac{YC}{\sqrt{CC}}$ and $\frac{YS}{\sqrt{SS}}$, respectively. The sign of these components is not yet known since shifting each t_n by τ introduces a phase shift. The phase shift can be accounted for by scaling the real and imaginary components of the Fourier transform by $\exp\{-i\omega_j[t_f - \tau(\omega_j)]\}$ where $t_f = 0$ for univariate analysis and

$$t_f = \frac{1}{N_x}\sum_{n=1}^{N_x} t_{x,n} - \frac{1}{N_y}\sum_{n=1}^{N_y} t_{y,n} \tag{A28}$$

for bivariate analysis. In practice, t_f accounts for time series data with different time origins.

To summarize, the least squares Fourier transform is given as

$$Y_j = \frac{1}{\sqrt{2}}\exp\{-i\omega_j(t_f - \tau)\}\left(\frac{YC}{\sqrt{CC}} + i\frac{YS}{\sqrt{SS}}\right) \tag{A29}$$

where τ is given as

$$\tau = \frac{1}{2\omega_j}\tan^{-1}\left[\frac{\sum_{n=1}^{N}\sin(2\omega_j t_n)}{\sum_{n=1}^{N}\cos(2\omega_j t_n)}\right]. \tag{A30}$$

Substituting YC, CC, YS, and SS into Eq. A29 gives

$$Y(\omega_j) = \frac{1}{\sqrt{2}}\exp\{-i\omega_j(t_f - \tau)\}\sum_{n=1}^{N}\left\{\frac{y_n\cos[\omega_j(t_n-\tau)]}{\sqrt{\sum_{n=1}^{N}\cos^2[\omega_j(t_n-\tau)]}} + i\frac{y_n\sin[\omega_j(t_n-\tau)]}{\sqrt{\sum_{n=1}^{N}\sin^2[\omega_j(t_n-\tau)]}}\right\} \tag{A31}$$

Approved for public release; distribution unlimited.